

<https://helda.helsinki.fi>

In vitro Evaluation of the Therapeutic Effects of Dual-Drug Loaded Spermine-Acetalated Dextran Nanoparticles Coated with Tannic Acid for Cardiac Applications

Torrieri, Giulia

2022-01-26

Torrieri , G , Almeida Ferreira , M , Shahbazi , M-A , Talman , V , Karhu , T , Pohjolainen , L , Carvalho , C , Pinto , J F , Hirvonen , J , Ruskoaho , H , Balasubramanian , V & Santos , H A 2022 , ' In vitro Evaluation of the Therapeutic Effects of Dual-Drug Loaded Spermine-Acetalated Dextran Nanoparticles Coated with Tannic Acid for Cardiac Applications ' , Advanced Functional Materials , vol. 32 , no. 5 , 2109032 . <https://doi.org/10.1002/adfm.202109032>

<http://hdl.handle.net/10138/341742>

<https://doi.org/10.1002/adfm.202109032>

cc_by_nc

publishedVersion

Downloaded from Helda, University of Helsinki institutional repository.

This is an electronic reprint of the original article.

This reprint may differ from the original in pagination and typographic detail.

Please cite the original version.

In Vitro Evaluation of the Therapeutic Effects of Dual-Drug Loaded Spermine-Acetalated Dextran Nanoparticles Coated with Tannic Acid for Cardiac Applications

Giulia Torrieri, Mónica P. A. Ferreira, Mohammad-Ali Shahbazi, Virpi Talman, S. Tuuli Karhu, Lotta Pohjolainen, Cláudia Carvalho, João F. Pinto, Jouni Hirvonen, Heikki Ruskoaho, Vimalkumar Balasubramanian,* and Hélder A. Santos*

Myocardial infarction results in a massive loss of cardiomyocytes (CMs). Unfortunately, current therapies are unsuccessful in replacing lost CMs, and thus, there is an urgent need for innovative approaches. Here, a nanosystem based on spermine-acetalated dextran (AcDXSp) and encapsulating two drug compounds able to stimulate in vitro CMs proliferation is developed. The nanosystem is coated by deposition of a film constituted by tannic acid (TA) and Fe³⁺ ions. The coating with TA increases the retention of the nanocarrier in cell co-cultures of CMs and fibroblasts stimulated with transforming growth factor (TGF)- β , due to the high affinity of TA for components of the cardiac extracellular matrix. The system exhibits biocompatibility toward primary CMs and induces their proliferation, as indicated by the two-fold increase of CMs in the active cell cycle. At the same time, the presence of TA synergistically helps contrasting fibrosis by reducing profibrotic genes expression, such as collagen 1 and osteopontin, by approximately 80% compared to the control. Overall, the developed nanosystem demonstrates the capability to stimulate CMs proliferation and reduce fibrosis, showing potential benefits for future in vivo applications.

and instead, initiates forming a scar.^[2,3] After that, the tissue goes toward a pathological remodeling of the left ventricular wall associated with hypertrophy, and fibrosis develops.^[3,4] The deposition of fibrotic tissue and the consequent hypertrophy of the cardiac muscle results in a progressive loss of contractile function, eventually leading to heart failure (HF).^[3] HF is a leading cause of mortality and morbidity, showing increasing prevalence with the aging of the population, and thus, representing a major public health issue.^[5]

Current therapies, unfortunately, cannot revert the pathological changes following a MI. They mainly help to contain the symptoms of the disease, but offer only small prolongations in survival.^[5] Hence, novel strategies to tackle HF and reduce mortality and morbidity are needed. A promising strategy for HF therapy could


be the inhibition of fibrosis, while stimulating cardiomyocytes (CMs) proliferation.^[3] The compounds used for the stimulation of CM proliferation include p38 mitogen-activated protein kinase (MAPK) inhibitors, like SB203580, and Wnt activators, such as CHIR99021.^[6] Inhibition of p38 MAPK up-regulated

1. Introduction

Myocardial infarction (MI) is one of the leading causes of death worldwide.^[1] Upon infarction, the heart cannot deal with the massive loss of cells by replacing it with new, functional CMs,

G. Torrieri, M.-A. Shahbazi, V. Talman, S. T. Karhu, L. Pohjolainen, J. Hirvonen, H. Ruskoaho, H. A. Santos
Drug Research Program
Division of Pharmaceutical Chemistry and Technology
Faculty of Pharmacy
University of Helsinki
Helsinki FI-00140, Finland
M. P. A. Ferreira
Bluepharma – Indústria Farmacêutica
São Martinho do Bispo
Coimbra 3045-016, Portugal

M.-A. Shahbazi
Department of Pharmaceutical Nanotechnology
School of Pharmacy
Zanjan University of Medical Sciences
Zanjan 56184-45139, Iran
M.-A. Shahbazi, H. A. Santos
Department of Biomedical Engineering and W.J. Kolff Institute for Biomedical Engineering and Materials Science
University Medical Center Groningen
University of Groningen
A. Deusinglaan 1, AV Groningen 9713, The Netherlands
E-mail: h.a.santos@umcg.nl
C. Carvalho, J. F. Pinto
Faculty of Pharmacy
University of Lisbon
Lisbon 1649-003, Portugal
V. Balasubramanian
Chemical and Pharmaceutical Development
Bayer Oy
Turku FI-20210, Finland
E-mail: vimalkumar.balasubramanian@helsinki.fi

 The ORCID identification number(s) for the author(s) of this article can be found under <https://doi.org/10.1002/adfm.202109032>.

© 2021 The Authors. Advanced Functional Materials published by Wiley-VCH GmbH. This is an open access article under the terms of the Creative Commons Attribution-NonCommercial License, which permits use, distribution and reproduction in any medium, provided the original work is properly cited and is not used for commercial purposes.

DOI: 10.1002/adfm.202109032

cell cycles specific genes, such as cyclin A, and genes involved in mitosis and cytokinesis, including cyclin B, cyclin-dependent kinase 2 (cdc2), and aurora B.^[7] Moreover, it regulates karyokinesis of neonatal CMs by increasing almost 4-fold the percentage of phospho-histone H3 positive CMs.^[7] Wnt/ β -catenin signaling has a pivotal role during the neonatal heart development, and in particular, it promotes cardiac differentiation at early developmental stages, while it inhibits it later.^[8] Activation of the Wnt pathway leads to inhibition of the glycogen synthase kinase 3 (GSK3) and this prevents degradation of β -catenin in the cytoplasm.^[9] CHIR99021 was identified as the most potent small-molecule compound able to stimulate human CM proliferation, inducing cell cycle activity marked by Ki67, and an increase in CM numbers compared to controls.^[10] Application of these therapies holds promises for the regeneration of the damaged heart. However, the administration of drugs able to induce cell proliferation could be a dangerous approach, since it could develop malignancies in other parts of the body.^[11] Also, it has been shown that, for example, long-acting miRNA gene therapy, despite having promising effects on the recovery of cardiac function after MI, resulted in lethal arrhythmias with death of the treated animals.^[12]

Moreover, the existing enhancers of CMs proliferation, such as small molecules, transcription factors, and miRNAs, suffer from poor bioavailability due to their hydrophobicity and/or instability.^[11]

Nanomedicine has brought promising innovations in the drug delivery field and can prevent the undesired effects arising from uncontrolled CMs proliferation. Many treatments have gained better efficacy as a result of the ability of engineered carriers to reach different parts of the body.^[13,14] Consequently, nanoparticles (NPs) are limiting systemic adverse effects of the therapeutic payloads, and moreover, they can allow delivery of multiple compounds.^[13,14] In recent years, there has been an increasing interest in nanomedicines for the treatment of cardiovascular diseases and many approaches have been proposed for heart targeting.^[15–19] Passive targeting was achieved by taking advantage of the leaky vasculature in the infarcted myocardium,^[20,21] as well as by developing materials that are responsive to mechanical and enzymatic stimuli.^[21,22] In particular, Hong et al. have recently developed NPs coated with low molecular weight heparin to achieve delivery of miR-1 into infarcted hearts, resulting in improved cardiac function and reduction of fibrosis.^[21] Active targeting instead, was accomplished by modifying the NPs surface with antibodies^[23,24] and different peptides,^[21,24] including a peptide targeting the angiotensin II type 1 receptor (AT1)^[15] and cyclic peptides like peptide CSTSMLKAC^[24] and CRSWNKADNRSC.^[19] In our group, different heart-targeting strategies have been exploited in the past, including the use of atrial natriuretic peptide (ANP) alone,^[25] or together with TT1 peptide, to achieve synergistic hitchhiking effect of macrophages.^[18] Moreover, NPs were loaded with compounds aiming at fibroblasts reprogramming,^[25] stimulation of CMs proliferation,^[18] and cardioprotection.^[17] However, the cardiac tissue with its constant pumping prevents the retention of nanocarriers in situ,^[26] and thus, there is an urgent need of molecules able to keep the nanocarriers long enough in the infarcted tissue.

Recently, Shin et al.,^[26] discovered that tannins can promote heart targeting and retention in place, as a result of the strong interaction with highly abundant components of the cardiac extracellular matrix (ECM), such as elastin and collagens. These interactions are dictated by the formation of multiple hydrogen bonds and hydrophobic interactions between the proteins in the ECM and the phenolic hydroxyl-rich moieties of tannic acid (TA).^[26]

Here, we exploited the heart targeting properties of TA by using it as a film to coat spermine-acetalated dextran (AcDXSp) NPs, which were used to improve the solubility of two small hydrophobic compounds, CHIR99021 and SB203580 that had been reported to stimulate CM proliferation.^[6]

We hypothesized that the TA coating enhances the interaction of AcDXSp NPs with cardiac cells, especially when cells are stimulated to produce more ECM. Also, the pH-responsive degradation of the TA coating could allow for sustained release of the compounds encapsulated. Moreover, the antifibrotic properties of TA could help reducing the expression of profibrotic genes in fibroblasts (FBs). Finally, the release of the small hydrophobic compounds for CM proliferation can induce increase of expression of proliferative markers in CMs, like Ki67 and phospho-histone H3, as well as, allowing complete cell division of CMs. The main goal of this study was to evaluate if the TA-coated AcDXSp could be used to target CMs and stimulate their proliferation, and fibroblast to inhibit fibrosis.

2. Experimental Section

2.1. Preparation of AcDXSp NPs and Coating with TA

AcDXSp NPs were prepared as described in Supporting Information. After collection and washings, the particles were coated with TA, as described in literature.^[28] Briefly, 0.5 mg of NPs were resuspended in 490 μ L of Milli-Q water pH > 8 and 5 μ L of a TA solution 40 mg mL⁻¹ were added and vortexed vigorously for 10 s. Subsequently, 5 μ L of an Fe³⁺ solution 6 mg mL⁻¹ were added to the suspension and vortexed for 10 s. Particles were then collected by centrifugation for 5 min at 13 400 \times g and washed once with Milli-Q water, pH > 8. All supernatants were kept for detection of the drugs, CHIR99021 and SB203580, using high-performance liquid chromatography (HPLC), as described below.

2.2. Indirect Determination of TA and Fe³⁺ Present in the Coating

After TA coating, the particles were centrifuged, as described above, and the supernatant was stored to determine indirectly the amounts of TA and Fe³⁺ present in the coating. Before any quantification, the supernatant was acidified with HCl 1 M to destroy the coordination complex.

The amount of TA present in the coating was determined indirectly by Folin-Ciocalteu's method.^[34] Briefly, 100 μ L of supernatant from the TA coating process were mixed with 200 μ L of Folin-Ciocalteu's reagent and vortexed vigorously. Then, 800 μ L Na₂CO₃ (700 \times 10⁻³ M) were added into each tube and incubated at room temperature for 2 h. Finally, absorbance at 765 nm was measured with a Varioskan Flash Multimode

Reader (Thermo Fisher Scientific). The amount of TA in the coating was determined by the difference between the total amount of TA added for the coating and the amount of TA found in the supernatant discarded after the coating. Fe³⁺ was instead determined by thiocyanate colorimetry.^[35] Briefly, 100 µL of ammonium thiocyanate solution (1 M) were added to 100 µL of acidified supernatant from the TA coating. After 15 min of incubation at room temperature, absorbance at 490 nm was measured with a Varioskan Flash Multimode Reader (Thermo Fisher Scientific). The amount of Fe³⁺ present in the coating was determined in indirect way, similarly to the TA.

2.3. Cell Cultures

All cell isolation, culture, and differentiation protocols are described in the Supporting Information.

2.4. Quantitative Uptake Studies on Primary Cardiac Cells and Primary M1- and M2-Like Macrophages

Primary rat cardiac cells were seeded onto six-well plates at a density of 5×10^5 and 1.5×10^5 cells per well for CMs and non-myocytes, respectively, and let to attach overnight at 37 °C. Cells were then incubated with 50 µg mL⁻¹ of fluorescent-labeled NPs for 2 h. After incubation, cells were washed twice with phosphate buffer saline (PBS)–ethylenediaminetetraacetic acid (EDTA), collected by trypsinization, and then washed again. All cells were finally dispersed in PBS–EDTA and quantitative uptake was evaluated by an LSR II flow cytometer (BD Biosciences, USA). In order to quantify the cellular uptake, external fluorescence was quenched by incubation for 4 min with trypan blue (TB; 0.005% v/v). Cells were then pelleted by centrifuging, dispersed in fresh PBS–EDTA and samples were run again.

Uptake of bare AcDXSp and TA-coated NPs was evaluated also on primary murine M1- and M2-like macrophages obtained by differentiation of monocytes isolated from bone marrows, as described in Supporting Information. The uptake of TA NPs also on these cells was evaluated to demonstrate that the TA coating has an antifouling effect, similar to PEG.^[26,31] Similarly, as described above, cells were seeded in six-well plates at a cell density of 5×10^5 cells per well. Fluorescently labeled NPs (50 µg mL⁻¹) were then incubated with the cells for 2 h. After incubations, cells were washed twice with PBS–EDTA and then detached by incubating them for 15 min on ice with a solution of PBS–EDTA with EDTA concentration of 3×10^{-3} M. The cell suspension was then evaluated by a BD Accuri C6 Plus (BD, USA) flow cytometer. All data were analyzed with FlowJo software (Tree Star, Inc., USA) and results were reported as MFI values.

2.5. Mechanism of Uptake Studies

The endocytosis mechanism adopted by cells to uptake AcDXSp-TA NPs was studied for both primary CMs and FBs. Before incubation with AcDXSp-TA NPs, cells were treated with the compounds listed in Table S1 (Supporting Information), in order to inhibit specific uptake pathways, and thus, evaluate the mechanism of internalization of the NPs. Incubation with the compounds was performed for 30 min, followed by the addition of AcDXSp-TA NPs. After incubation, cells were washed, detached, dispersed in PBS–EDTA and analyzed by flow cytometry, as described above.

2.6. Qualitative Uptake Studies

Qualitative uptake studies were performed by confocal imaging on primary CMs, FBs, and co-cultures of the previous cell lines, both with and without TGF-β stimulation. Cells were seeded in eight-well chambers (Lab Tek™, Thermo Fisher Scientific, USA) pre-coated with gelatine. Cell co-cultures were settled up by seeding directly the cell suspension obtained after tissue digestion. After seeding, cells were let attach overnight and then they were treated with TGF-β at a concentration 3 ng mL⁻¹ for 48 h. Subsequently, cells were incubated with 50 µg mL⁻¹ of fluorescently labeled NPs for 2 h. After treatment with AcDXSp and AcDXSp-TA NPs, cells were washed 2 × 5 min with PBS, fixed for 20 min with a solution of paraformaldehyde (PFA) at a concentration of 4% (v/v) and then washed again 3 × 5 min with PBS. After fixation, immunostainings were carried out. Some wells were left untreated to characterize the three different cell cultures. First, cells were permeabilized with 0.1% (w/v) Triton X-100, then washed 2 × 5 min with PBS and blocked with 4% (v/v) FBS in PBS for 45–60 min. Incubation with primary antibodies for 60 min at room temperature, shaking at 300 rpm was then following. Different cells were treated with different antibodies according to the scheme presented in Table 1.

Afterward, cells were washed 3 × 5 min with PBS and then secondary antibodies (anti-rabbit 546 (1:250, A-11035), anti-mouse 488 (1:250, A11029), anti-rat 647 (1:200, A-21247) (all from Invitrogen, USA), and DAPI, (1:250, Vector Laboratories) were added to each well and incubated for 45 min at room temperature, shaking at 300 rpm. Cells were washed 3 × 5 min with PBS and stored in darkness at +4 °C in Ibidi glycerol-based mounting media until imaging (Ibidi, Germany). Images were captured by using a 63 × glycerol objective in a Leica TCS SP8 STED 3X CW 3D inverted microscope (Leica Microsystems, Germany) and then processed with Leica AS software (Leica Microsystems, Germany).

Table 1. Primary antibodies used in qualitative uptake studies.

	Cardiomyocytes	Fibroblasts	Coculture
Uptake samples	Rabbit anti-Collagen I (1:500, ab34710, Abcam)	Rabbit anti-Collagen I (1:500, ab34710, Abcam)	Rabbit anti-Collagen I (1:500, ab34710, Abcam)
Characterization samples	Rabbit anti-Collagen I (1:500, ab34710, Abcam), mouse anti-cTnT (1:500, MS_295, ThermoFisher Scientific)	Rabbit anti-Collagen I (1:500, ab34710, Abcam), rat anti-Vimentin (1:250, MAB2105, Rndsystem)	Rabbit anti-Collagen I (1:500, ab34710, Abcam), mouse anti-cTnT (1:500, MS_295, ThermoFisher scientific), rat anti-Vimentin (1:250, MAB2105, Rndsystem)

2.7. Determination of Cell Proliferation: Ki67, Phospho-Histone H3, and Aurora B Kinase Immunostainings

For the determination of proliferation, primary CMs were seeded in transparent 96-well plates (Corning, USA) at a cell density of 2.5×10^4 cells per well and left to attach overnight. Ki67 immunostainings were performed also on hiPSC-CMs and in that case, cells were seeded at a cell density of 2.5×10^4 cells per well. hiPSC-CMs were obtained, as described in Supporting Information, and they were at day 20 post-differentiation when treated with the NPs. Cells were then treated with different concentrations of empty and loaded AcDXSp and AcDXSp-TA NPs corresponding to concentrations of CHIR99021 of 1×10^{-6} , 3×10^{-6} , 5×10^{-6} and 10×10^{-6} M (calculated according to loading degree (LD) values). Compounds alone, were used as positive controls, while medium alone and medium containing 1% (v/v) DMSO, were used as controls for empty and drug-loaded NPs. After 24 h, cells were placed on ice to block all cellular actions, washed twice with PBS pH 7.4 and then fixed for 20 min with a solution of PFA at a concentration of 4% (v/v). After fixation, cells were washed 3×5 min with PBS and then permeabilized for 10 min with 0.1% (w/v) Triton X-100. Then cells were washed 2×5 min with PBS and blocked with 50 μ L of 4% (v/v) FBS in PBS for 45–60 min. FBS was removed and cells were incubated with 30 μ L of primary antibodies (Rabbit Anti-Ki67 antibody [SP6] (1:200, ab16667, Abcam), Rabbit Anti-Phospho-Histone H3 (Ser10) (1:500, 9701S, Cell Signaling Technology), Rabbit Anti-Aurora B (1:500, ab2254, Abcam) and Mouse Anti-troponin T, cardiac (1:500, MS_295, ThermoFisher scientific)) for 60 min at room temperature, shaking at 300 rpm. Aurora B and phospho-histone H3 immunostainings were performed by incubating cells with primary antibodies overnight at +4 °C. Primary antibodies were washed away 3×5 min with PBS and 30 μ L of secondary antibodies (goat anti-mouse IgG H+L Alexa-546 (1:250, A-11030, Life Technologies; donkey anti-rabbit IgG H+L Alexa-647 (1:250, A-31573, Life Technologies) and DAPI (1:250, Vector Laboratories) were added for 45–60 min at room temperature, shaking at 300 rpm. Wells were also treated with medium and used as a secondary antibody control. Cells were finally washed 3×5 min with PBS and stored in darkness at +4 °C until imaged. Plates were then imaged with an ImageXpress Nano (Molecular Devices, USA) high content imaging system using a 10 \times objective. Analysis was conducted with a MetaXpress 6.6.1.42 software (Molecular Devices).

For quantification, the cells were first identified based on DAPI fluorescence, which defined the nuclear area. Non-myocytes were excluded based on the absence of cardiac troponin T staining. The threshold for cardiac troponin T fluorescence intensity was set manually in each experiment to allow optimal exclusion of non-myocytes. The data were collected only from cardiac troponin T-positive cells. The intensities of Ki67, phospho-histone H3 and aurora B stainings were analyzed within the nucleus. The threshold for Ki67, phospho-histone H3, and aurora B positive cells was set manually in each experiment to adjust for minor variation in staining intensity. For aurora B immunostainings, analysis of the surface area of CMs by identifying and quantifying the area of cTnT staining was also run. The percentage of CMs in telophase was obtained

by manually counting in a blinded experiment the number of cells that were presenting the aurora B staining between the two dividing cells. Percentages were then calculated referring to the total amount of CMs present in each well (calculated by the MetaXpress 6.6.1.42 software).

2.8. Real-Time Quantitative Polymerase Chain Reaction (RT-qPCR) Studies

The anti-fibrotic effect of TA and the proliferative effect of drug-loaded NPs were evaluated by RT-qPCR. Primary rat FBs and CMs were seeded in six-well plates (Corning, USA) at a cell density of 2.5×10^5 and 5×10^5 cells per well, respectively, and let to attach overnight. Empty and loaded NPs, as well as compounds alone, were added to the cells in order to achieve a concentration of CHIR99021 of 3×10^{-3} M, based on the LD of the NPs. Cells were treated also with medium and medium containing 1% (v/v) of DMSO as controls. After 24 h incubation, RNA was isolated from cells using TRIzol reagent (Invitrogen), following the manufacturer's protocol by using the Phase Lock Gel system (Eppendorf AG). The cDNA was synthesized from total RNA with a First-Strand cDNA Synthesis Kit (GE Healthcare Life Sciences), following the manufacturer's instructions. Finally, the RNA was analyzed by RT-PCR on a LightCycler 480 qPCR machine (GE Healthcare Life Sciences) using TaqMan chemistry. The results were quantified using $\Delta\Delta$ CT method and normalized to housekeeping gene *18S* quantified from the same samples. The following pre-designed TaqMan probes from Thermo Fisher Scientific were used in the assay: *18S* (4352930E), *Col1a1* (Rn01463848_m1), *Spp1* (Rn00681031_m1), *Tgfb1* (Rn00572010_m1), *Tnfa* (Rn01525859_g1), *Myc*(Rn07310910_m1) *Fos*(Rn02396759_m1), *Ccna2*(Rn01493715_m1), *Ccnb1* (Rn01494180_g1), *Ccnd1* (Rn00432359_m1) and *Ccne1* (Rn01457762_m1).

2.9. Statistical Analysis

Statistical analysis was performed using a GraphPad Prism 7 (GraphPad Software, Inc., La Jolla, CA, USA). The statistical methods used to analyze the data from each experiment are described in each figure caption.

3. Results and Discussion

3.1. Nanoparticles Synthesis and Physicochemical Characterization

The AcDXSp NPs were prepared by oil-in-water (o/w) single emulsion technique, as previously described,^[25] and the compounds to stimulate CMs proliferation, CHIR99021 and SB203580 (abbreviated respectively as CHIR and SB for simplification), were dissolved in the organic solvent together with the spermine-acetalated dextran polymer during the emulsion formation. Then, coating was obtained by sequential addition, followed by vortexing of solutions of TA with Fe³⁺,

as described by Guo et al.^[27] The coating changed the color of the NPs suspension from white to grey (Figure S1, Supporting Information). This resulted in the formation of coordination bonds, which allowed the TA film formation and deposition in a pH-dependent manner.^[28] The coating took place in a few second time, allowing for a fast and easy surface modification of the NPs, a more advantageous approach compared to the different and time-consuming conjugation steps usually used to conjugate moieties on the NPs surface. Fe³⁺ was chosen considering its adhesive properties after coordination with polyphenolic materials.^[29] The presence of Fe³⁺ in the coating can also be exploited for magnetic resonance imaging purposes in the future, enabling to follow the NPs fate inside the body.^[30] Moreover, TA demonstrated to be able to increase the stability of NPs in blood circulation, increasing their circulation time, similarly as polyethylene glycol (PEG).^[26,31]

The bare and TA-coated NPs were then characterized by dynamic light scattering (DLS) and electrophoretic light scattering (ELS) (Figure 1A). The concentrations and ratios of TA and Fe³⁺ were previously optimized by monitoring the particle size and polydispersity index (PDI) values of the obtained nanosuspensions (data not shown). We finally chose the optimal condition that produced NPs with the smallest size and PDI values as possible. This is important for future in vivo applications, since the size of NPs, among other aspects, affects their circulation in the bloodstream.^[32]

As shown in Figure 1A, there was an increase in size of the NPs after coating, which is hypothesized to be due to the

deposition of the coordination complex made of TA and Fe³⁺ on the NPs. Moreover, the change of zeta-potential charge from positive to negative values after coating with TA, provided evidence of the presence of TA coating on the NPs' surface. Empty and loaded NPs did not show any significant difference in size or surface charge among them.

Further confirmation of the presence of TA and Fe³⁺ in the coating of the produced NPs was evaluated by KBr Fourier-transform infrared (FT-IR) spectroscopy of the different components alone and the NPs before and after coating. As shown in Figure 1B, after deposition of the TA-Fe³⁺ coordination complex on the NPs' surface, bands corresponding to the carbonyl groups C=O stretching (1714 cm⁻¹) appear in the spectrum, as well as a broadening of the band corresponding to the stretching of the hydrogen bonds established by the hydroxyl groups (O-H).^[33]

Furthermore, we studied the morphology of the nanosystem by acquiring transmission electron microscopy (TEM) images, which showed the presence of an irregular coating on the NPs surface after the addition of TA and Fe³⁺ (Figure 1C,D). The amounts of TA and Fe³⁺ in the coating of AcDXSp NPs were determined indirectly by Folin Ciocalteu's method^[34] and isothiocyanate colorimetry,^[35] respectively. In 1 mg of TA coated NPs there were 167.3 µg of TA and 10.5 µg of Fe³⁺ on the surface.

Considering that all in vitro studies were performed in cell medium, we determined the colloidal stability of the nanosystems in Dulbecco's modified Eagle's medium (DMEM)/F-12 containing fetal bovine serum (FBS). We also evaluated their

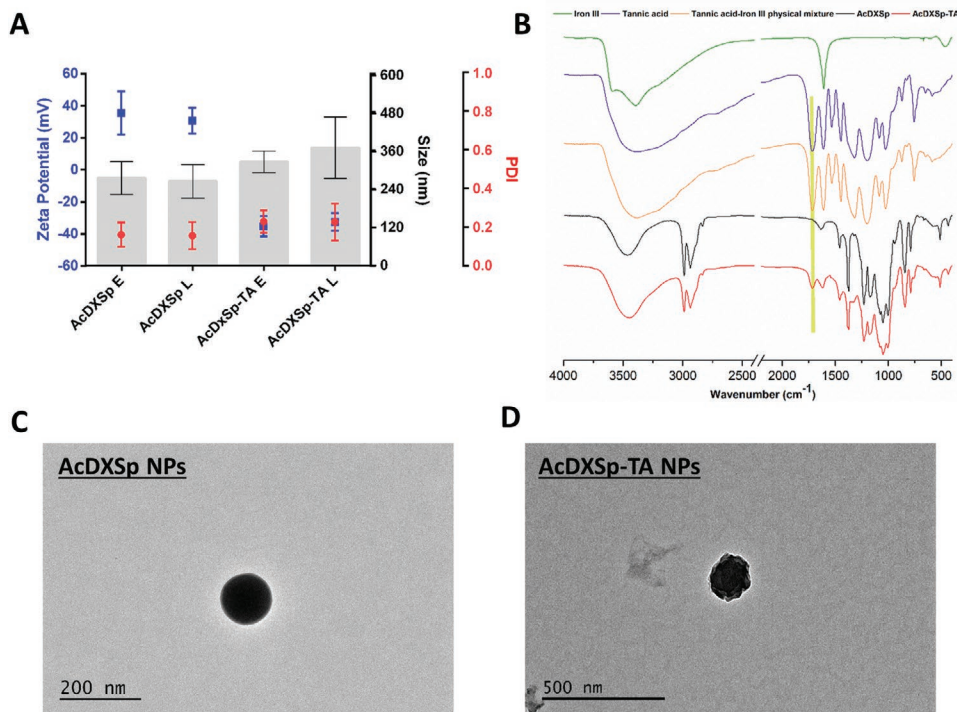


Figure 1. Physicochemical characterization of AcDXSp-TA NPs. NPs were characterized by DLS and ELS to obtain information about A) the particle size, PDI, and zeta-potential, B) KBr-FTIR for the chemical composition of the NPs' surface and representative TEM on the morphology of the NPs C) before and D) after coating with TA. Values are represented as the mean \pm standard deviation (s.d.) ($n \geq 3$ biological replicates in which each time three technical replicates have been used).

stability in human plasma for comparison. When NPs were tested in medium containing serum for 2 h, uncoated AcDXSp NPs showed an increase of size (Figure 2A) and PDI (Figure 2B) over time, while the TA-coated NPs were more stable. The same trend was recorded when the stability was performed in human plasma (Figure 2C). The stability was monitored also in an isotonic glucose solution, considered as a vehicle to resuspend the NPs during injections for future in vivo applications. Also in isotonic glucose solution, the NPs showed very good stability in terms of size and PDI (Figure 2D,E), validating its potential use as NPs resuspension media for injections. Altogether, these results show the potential of TA coating to reduce the

interaction of coated AcDXSp NPs with plasma proteins and serum in vitro, showing similar properties to PEG.^[26,31]

3.2. Release Studies in PBS (pH 7.4) and in Acetate Buffer (pH 5.0)

The in vitro release profiles of CHIR and SB were evaluated in both PBS (pH 7.4) and acetate buffer (pH 5.0) to mimic the physiological extracellular environment and the conditions found in acidic intracellular compartments after internalization in the cells, respectively.^[36] The release of the drugs was evaluated

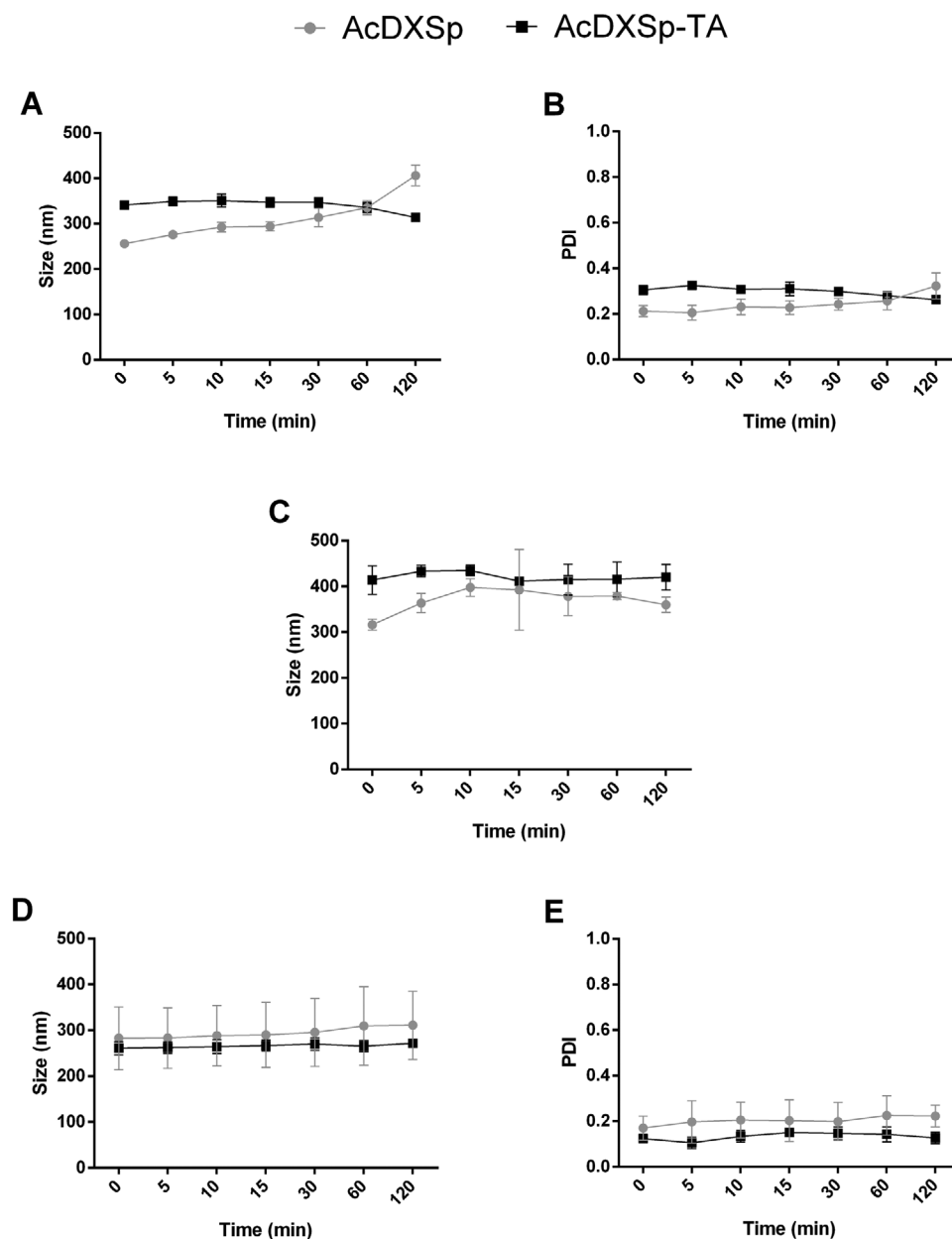


Figure 2. Evaluation of the colloidal stability of AcDXSp-TA NPs in different media. Stability studies were performed by A) recording size and B) PDI in DMEM F-12 + 10% FBS, C,D) glucose 5.4% (w/v) and E) in human plasma. Values are represented as the mean \pm standard deviation (s.d.) ($n \geq 3$ biological replicates in which each time three technical replicates have been used).

over 24 h, considering that this is the maximum incubation time with the NPs during the *in vitro* evaluation of CMs proliferation. Before determining the release profile of the two compounds, we also determined the loading degree (LD) and encapsulation efficiency (EE%) values for both uncoated and TA-coated AcDXSp NPs (Table S2, Supporting Information). The encapsulation of the drug molecules was done at a molar ratio CHIR:SB of 1:2, which is the optimal ratio, according to the literature, in order to induce CMs proliferation.^[7,37]

As shown in Figure 3A,B, SB displayed an increased release rate at pH 5.0 compared to pH 7.4. The same was noted for drug CHIR, of which less than 20% of drug released at pH 7.4 (Figure 3C), while more than 50% of the drug released at pH 5.0 (Figure 3D). This is in accordance with the pH-dependent hydrolysis of the acetal groups present in AcDEX.^[38–40] Free drugs were used as controls, and especially in the case of CHIR, the NPs increased its dissolution rate in aqueous media. Also, the solubility of CHIR was affected by the pH, where the free drug was more soluble at pH 5.0 (Figure 3D) than at pH 7.4 (Figure 3C). For SB at pH 5.0 (Figure 3B), it can be noticed the NPs improve the stability of the drug (the free drug dissolution decreased after 8 h, possibly due to degradation), whereas the drug-loaded NPs showed increase of the drug concentration up to 24 h.

The drug release was evaluated also in DMEM supplemented with 10% FBS and as shown in Figure 3E,F, the presence of serum enhanced the release of the compounds, in particular for CHIR (Figure 3F). The NPs coated with TA showed a slower release for both the compounds and this can be attributed to the pH-dependent disassembly of the TA-Fe³⁺ capsules.^[28] It has been demonstrated that at pH 2 TA capsules shrank immediately and disassembled, since at acidic pH most of the hydroxyl groups of TA are protonated and this leads to rapid destabilization of cross-links and disassembly of the films.^[28] At pH 5 and 7.4, instead, ≈70% and 90% of the capsules, respectively, remain intact after 10 days of incubation.^[28] Considering also that inflammation occurring in the ischemic myocardium lowers the interstitial pH to 6–6.5,^[41,42] these NPs could be used for the sustained release of cargos into the infarcted myocardium^[43] under these conditions. However, if a faster release is desired, the nanosystem can be easily tuned by just changing the metal used to form complexes with the TA, in order to fulfill the requested pH-responsive release.^[27]

3.3. Cell Viability Studies on Primary CMs and FBs

The cytocompatibility of the system was evaluated on human coronary artery endothelial cells (HCAECs) and primary neonatal rat cardiac cells by CellTiter-Glo luminescence assay, which detects the number of viable cells in culture based on quantitation of the ATP present.^[44] Cell viability was determined after incubation with the particles for 24 and 48 h with primary CMs and FBs and 6 and 24 h with HCAEC. The time-points were chosen considering the slow release of drugs from the NPs and the desired effect on CMs, produced by the compounds CHIR and SB (stimulation of CM proliferation by re-entry in the cell cycle). We screened different NP concentrations, including higher concentrations of NPs to evaluate how the concentration

range affects the safety. HCAEC were chosen considering that ideally these are the first cells encountered by the NPs when arriving to the cardiac tissue. As shown in Figure S2 (Supporting Information), empty AcDXSp and AcDXSp-TA NPs reduced the viability of HCAEC, especially after 24 h at higher doses (after 24 h the viability was around 50% and 40% for AcDXSp and AcDXSp-TA at a concentration of 500 μg mL⁻¹, respectively). This cytotoxicity was recovered by loaded NPs, probably due to the protective effect of the drugs.^[7,45] Similarly, as shown in Figure 4, AcDXSp NPs showed a dose-dependent cytotoxicity toward both primary CMs (Figure 4A,B) and FBs (Figure 4C,D), with stronger decrease of cell viability after 48 h (Figure 4B,D).

The cytotoxicity of AcDXSp NPs can be ascribed to their highly positive charge, which results in increased interaction with the negatively charged cell membranes, causing disruption of the plasma-membrane integrity, production of a high number of autophagosomes and damage to cellular organelles, in particular mitochondria and lysosomes.^[46] Loading with CHIR and SB, improved the safety of both nanocarriers, suggesting a protective effect of the drugs on the cells. However, considering the toxicity of the highest concentration of NPs, we would exclude such concentrations for therapeutic purposes.

The biocompatibility was also assessed by incubating primary cardiac cells with TA, Fe³⁺, and TA-Fe³⁺ for 24 and 48 h. In Figure S3 (Supporting Information), it is shown that primary CMs (Figure S3A,B, Supporting Information) are less sensitive compared to FBs (Figure S3C,D, Supporting Information), and this can be explained by the anti-fibrotic properties of TA.^[47,48] Fe³⁺, did not show statistically significant cytotoxicity differences in both CMs and FBs and when complexed with TA, improved the TA safety profile.

3.4. Cell–Nanoparticle Interactions with Primary Cardiac Cells

Interaction with cardiac cells was evaluated both quantitatively and qualitatively. For the quantitative uptake, cells were treated with fluorescently labeled NPs for 2 h and the uptake was evaluated by flow cytometry. Figure 5 shows the median fluorescence intensity (MFI) values for cells treated with both AcDXSp and AcDXSp-TA NPs. Both primary CMs (Figure 5A) and FBs (Figure 5B) showed more interaction with AcDXSp NPs compared to TA-coated NPs, possibly due to the fact that AcDXSp NPs are highly positively charged and more prone to interact with negatively charged cell membranes, as described previously for the cytocompatibility studies.^[46] However, TA-coated NPs still showed a statistically significant interaction with cells, showing that the TA coating is by no mean preventing the uptake of NPs by the cells. Moreover, no statistically significant differences were observed between MFI values before and after surface fluorescence quenching with trypan blue, meaning that NPs were mainly taken up by the cells. Furthermore, both TA coated and uncoated AcDXSp NPs exhibited preferential interaction with primary CMs, considering the higher MFI values.

The internalization mechanism was also studied by pre-incubating the cells with different endocytosis inhibitors. Cytochalasin D (CytoD) depolarizes actin filaments, and thus, was used to study the micropinocytosis and the role of actin

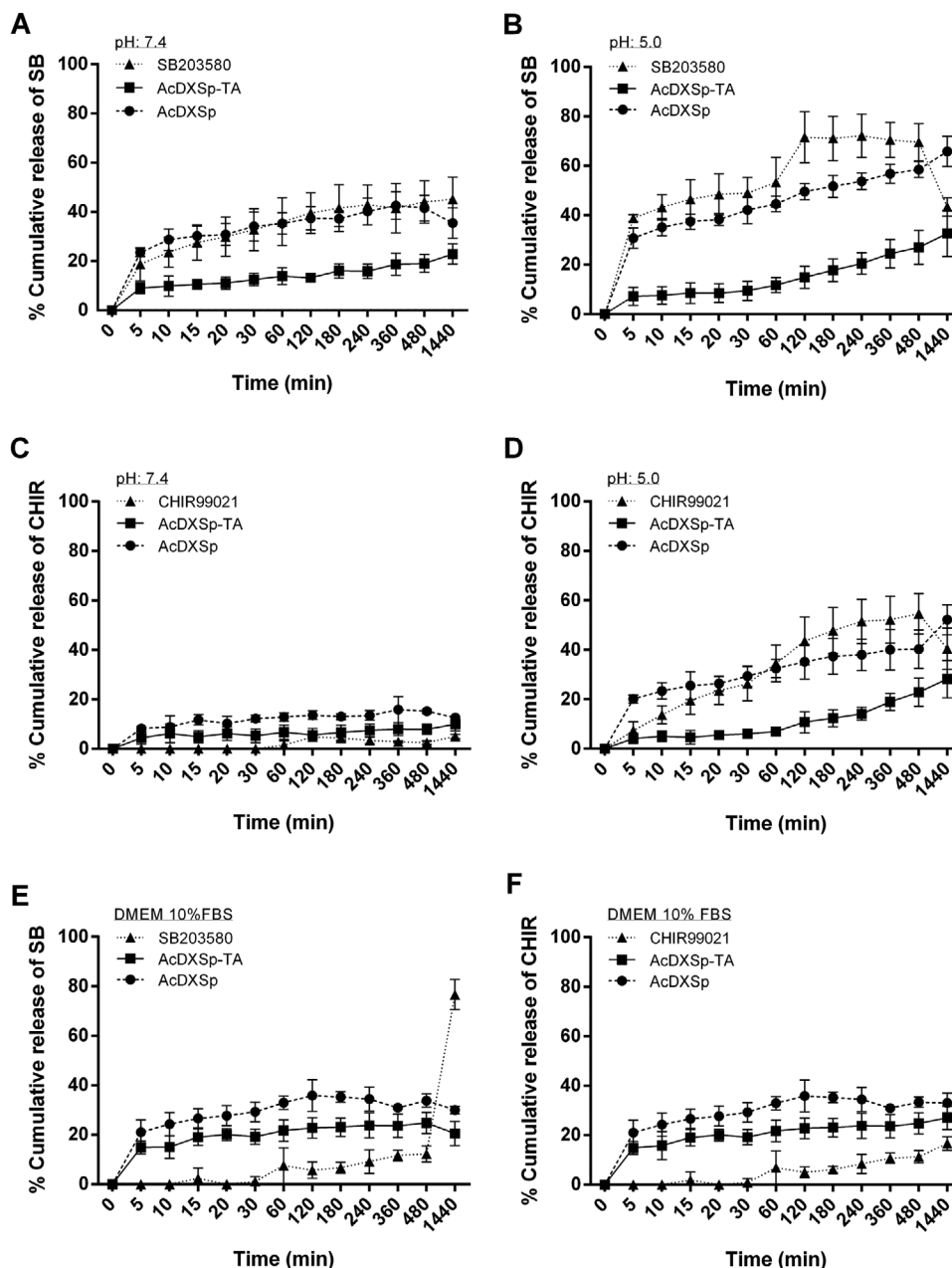


Figure 3. Release profiles of drug-loaded AcDXSp NPs. Release profiles of A,B,E) SB203580 and C,D,F) CHIR99021 from bare CS@AcDXSp and functionalized CS@AcDXSp-TA in PBS (pH 7.4), acetate buffer (pH 5.0) and in DMEM F-12 + 10% FBS at 37 °C. Data represented as mean \pm s.d. ($n \geq 3$ biological replicates in which each time three technical replicates have been used).

in the endocytic process.^[49,50] Genistein is an isoflavone, which has suppressive effects on tyrosine kinases involved in caveolin-mediated endocytosis.^[51–53] Clathrin-mediated uptake was inhibited by interference with clathrin disassembly and receptor recycling to the plasma membrane by chlorpromazine.^[54] Finally, sodium azide, since it interferes with ATP production due to its ability in inhibiting cytochrome c oxidase, was used to study particle uptake via active transport.^[55,56] As shown in Figure 5, both CMs (Figure 5C) and FBs (Figure 5D) exhibited the highest uptake inhibition after treatment with CytoD and sodium azide, suggesting that actin filaments were

the cytoskeleton components involved in the uptake mechanism of the AcDXSp-TA NPs, with the engagement of energy-dependent pathways.

Qualitative uptake studies were also performed on primary CMs, FBs, and cell co-cultures, and samples were analyzed using confocal microscopy. For these studies, cells were treated with TGF- β to stimulate ECM production, with the aim to mimic the fibrosis taking place after an infarction.^[3] Control cells were used to characterize both the cell cultures and co-cultures. As shown from the characterization images in Figure S4 (Supporting Information), after stimulation with

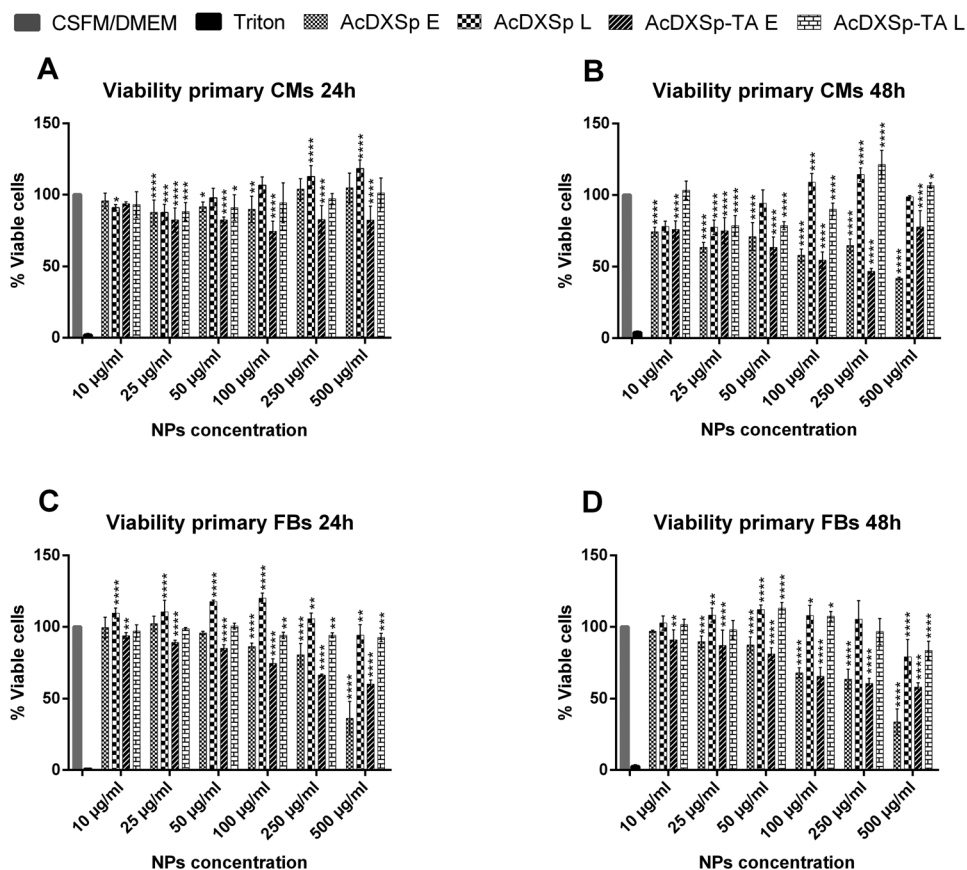


Figure 4. Cell viability of primary rat CMs and FBs. Cytocompatibility studies were conducted to assess the safety of the produced NPs on both primary rat A,B) CMs and C,D) FBs. Values are represented as mean \pm s.d. ($n = 3$ biological replicates in which each time three technical replicates have been used). A one-way ANOVA followed by a Tukey–Kramer post hoc test was used for the statistical analysis. The significance levels of the differences were set at the probabilities of $*p < 0.05$, $**p < 0.01$, $***p < 0.001$ and $****p < 0.0001$ for comparison with the medium, which was used as a control in all the tests.

TGF- β there is an increase of collagen I production, based on increased collagen I staining especially in FBs and cell co-cultures. CMs cultures, which contain none or very few FBs as contaminants, present a less dense collagen I production. Both CMs and FBs also exhibited morphological signs of hypertrophy, since stimulation with TGF- β is also involved in the hypertrophic and dilative ventricular remodeling by stimulating CM growth and by inducing interstitial fibrosis.^[57] After characterization of TGF- β stimulated cultures, we proceeded with uptake studies to evaluate if the ECM production, with higher collagen deposition, could enhance the retention of the NPs after modification with TA. As shown in **Figure 6**, TA-coated NPs interacted more than bare AcDXSp NPs with the cells, especially after treatment with TGF- β . These observations are in accordance with the finding that TA can achieve heart targeting due to its high affinity for components of the ECM.^[26] Interestingly, CMs cultures, which have less production of collagen I, compared to FBs and co-cultures, showed a relatively high amount of TA-coated NPs interacting with the culture and this could be in accordance with flow cytometry data showing that the TA-coated NPs were more interacting with CMs compared to FBs.

Altogether, these qualitative observations suggest that TA-coated AcDXSp NPs interact to a higher extent with TGF- β

stimulated cardiac cells co-cultures, possibly as a result of their affinity for the ECM.

Next, we performed uptake studies also on primary M1- and M2-like macrophages isolated from murine bone marrow, in order to evaluate the interactions of the NPs with the phagocytic system cells. Macrophages were assessed by determining their markers' expression, as shown in Figure S5 (Supporting Information). Considering that modification with TA has shown increased blood circulation time, similarly to PEG,^[26,31] we expected a reduction of such interaction. For this purpose, we evaluated the cell uptake after 2 h of incubation with the NPs. As shown in Figure S6 (Supporting Information), the TA-coated NPs are taken up to a less extent compared with bare AcDXSp NPs, demonstrating the stealth potential of AcDXSp NPs after TA coating.^[31]

3.5. Anti-fibrotic Effect of TA-Coated NPs

The anti-fibrotic properties of TA were exploited to contrast the fibrosis taking place after a MI.^[58] In this regard, we combined the proliferative effect of the encapsulated drugs together with the anti-fibrotic properties of the TA coating, aiming at a synergistic repair of the cardiac tissue. For this, we studied

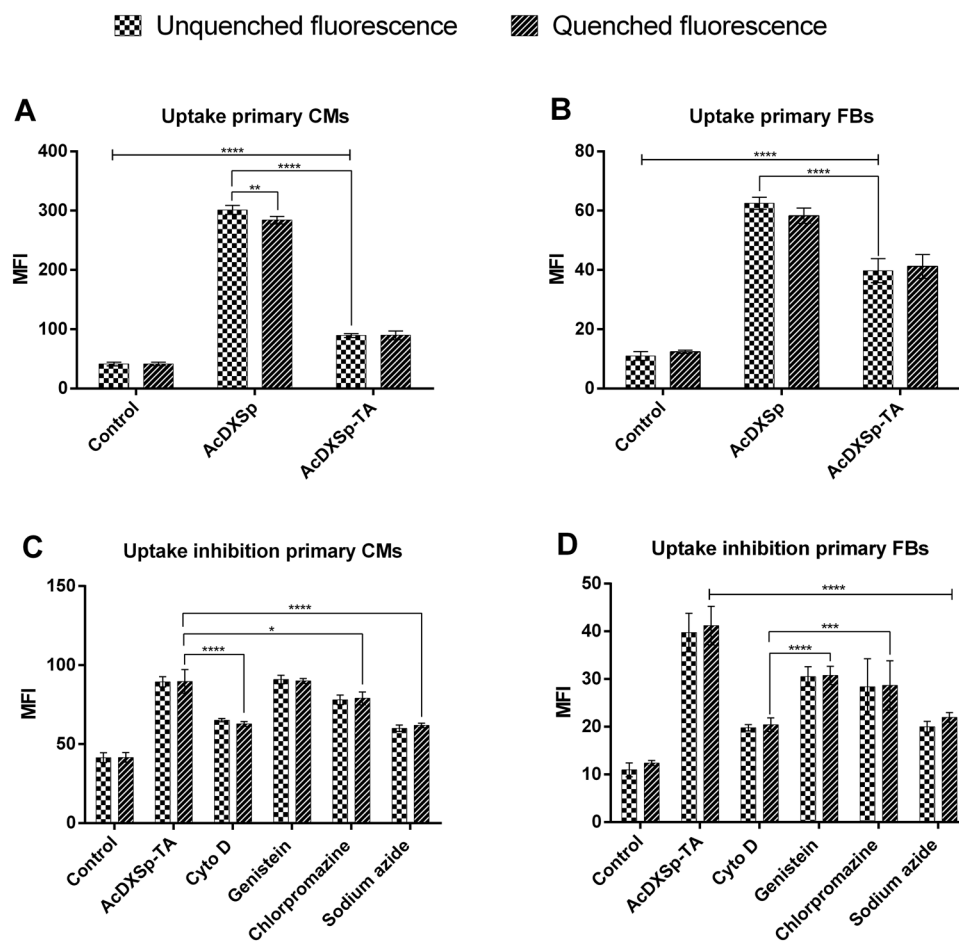


Figure 5. Quantitative cell uptake and uptake mechanisms studies on primary rat CMs and FBs. Interactions between AcDXSp-TA NPs and the cells were studied on primary rat A) CMs and B) FBs. Uptake mechanism was also studied on both C) CMs and D) FBs: cells were incubated with different compounds, each one inhibiting a different mechanism of endocytosis, and then particles were added and the cell uptake evaluated by flow cytometry. Results are represented as MFI values \pm s.d. ($n = 3$ biological replicates in which each time three technical replicates have been used). A one-way ANOVA followed by a Tukey–Kramer post hoc test was used for the statistical analysis. The significance levels of the differences in uptake studies were set at the probabilities of $**p < 0.01$ and $****p < 0.0001$ for comparison between associated and internalized AcDXSp NPs, before and after fluorescence quenching with trypan blue and between AcDXSp and AcDXSp-TA NPs, respectively. In uptake mechanism studies, the significance levels of the differences were set at the probabilities of $**p < 0.01$, $***p < 0.001$, and $****p < 0.0001$ for comparison between internalized AcDXSp-TA NPs and cells treated with different endocytosis inhibitors.

the effects of TA-coated NPs on reducing the expression of profibrotic genes in cardiac fibroblasts by real-time quantitative polymerase chain reaction (RT-qPCR). We chose to detect the expression of six pro-fibrotic genes (Col1a1, Tgfb, Fos, Myc, osteopontin (Spp1) and tumor necrosis factor- α (Tnfa)) in primary rat FBs, treated with NPs and drugs corresponding to a concentration of CHIR of 3×10^{-6} M (concentrations of SB were approximately double) for 24 h. We used the 18s gene as control housekeeping gene, while cell medium and DMSO were used as controls for the NPs and the drugs, respectively. Col1a1 gene has recently been recognized as marker in human heart failure progression, being its increase highly correlated to fibrosis and HF.^[59] TGF- β is considered to be the principal cytokine/growth factor secreted during fibrosis and activating fibroblasts in producing more ECM.^[60] Excessive expression of secreted phosphoprotein 1 Spp1^[61] and Fos^[62] genes are also directly correlated with fibrosis. The Myc oncogene is a

transcription factor with a wide array of functions affecting cellular activities, such as cell cycle, proliferation, and hypertrophy. TNF- α is a pro-inflammatory cytokine secreted after MI and it regulates the remodeling of the heart, promoting the advent of the pro-fibrotic response.^[63] As shown in **Figure 7**, the loaded TA-coated AcDXSp NPs were able to reduce the expression of Col1a1 (Figure 7A), Tgfb (Figure 7B), Spp1 (Figure 7C), Myc (Figure 7E), and Fos (Figure 7F) genes. In particular, the expression of genes such as Col1a1 (Figure 7A) and Spp1 (Figure 7C) was decreased by $\approx 80\%$ when cells were treated with drugs loaded AcDXSp-TA (AcDXSp-TA L) NPs.

For the Tnfa gene (Figure 7D), it was observed an increase of expression when cells were treated with drug-loaded AcDXSp-TA (AcDXSp-L) NPs. These results were not expected considering the reported anti-inflammatory properties of both TA^[64,65] and compounds encapsulated.^[66–70] However, according to some reports, TA could be able to induce an increase of

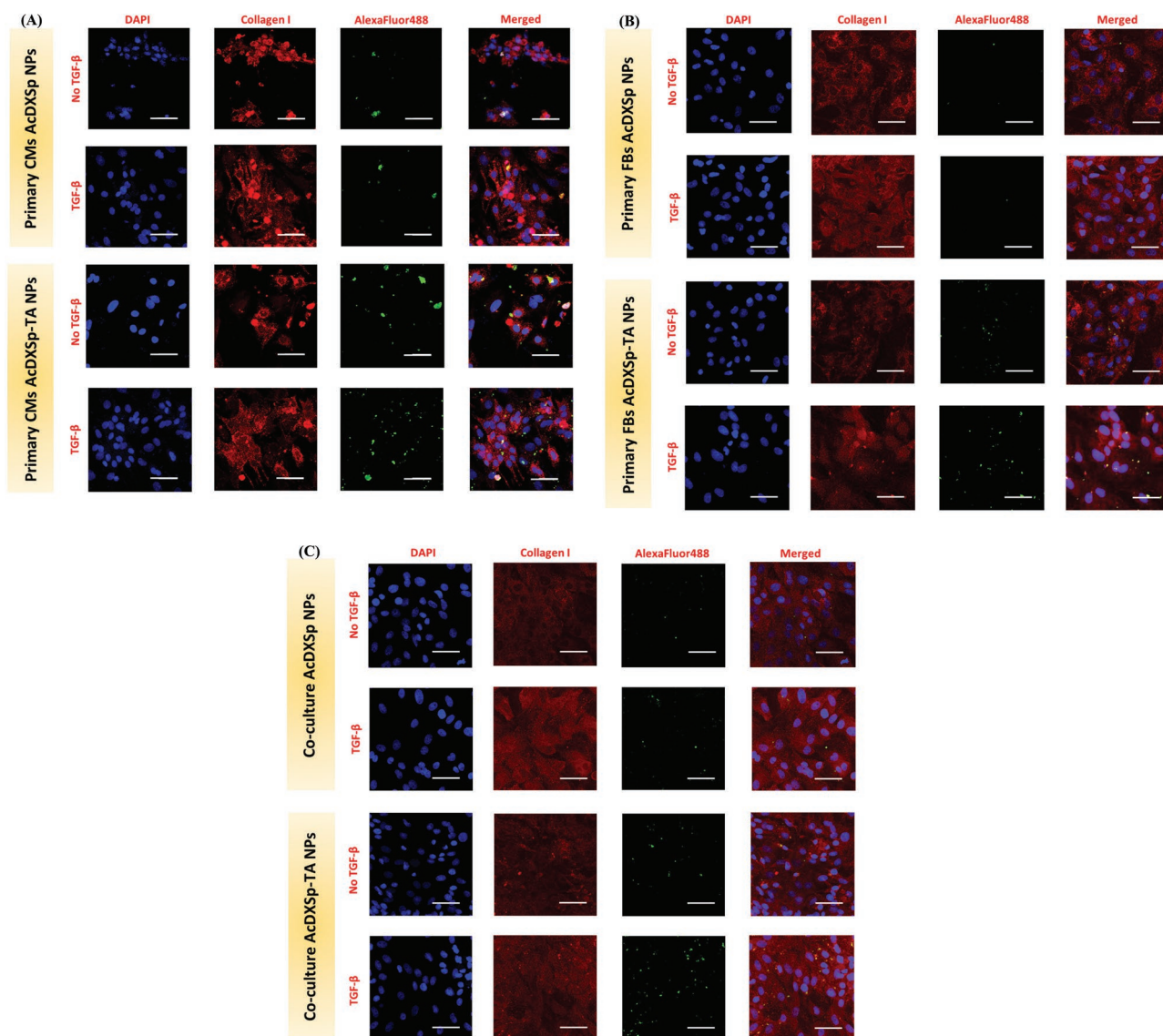


Figure 6. A–C) Qualitative uptake studies on primary rat CMs, FBs, and cell cocultures stimulated and nonstimulated with $TGF\beta$. The cell uptake was evaluated by confocal fluorescence microscopy after incubation with the NPs for 2 h at 37 °C. The NPs were conjugated with AlexaFluor488, while cells were stained with DAPI (nuclei) and anti-Collagen I antibody (collagen/ECM). Scale bars are equal to 50 μ m.

TNF- α in keratinocytes in patients affected by pemphigus vulgaris.^[71]

Altogether, the results demonstrate that the TA coating can inhibit the expression of pro-fibrotic genes and fibrosis markers in vitro and potentially have a synergistic effect for tissue repair when combined with the proliferative compounds encapsulated in the NPs.

3.6. Stimulation of Cardiomyocytes Proliferation

The ability of the nanosystem to induce cell division in CMs was also evaluated by investigating the proliferation in cardiac cells by fluorescent detection of different proliferation markers: Ki67,^[48,49] phospho-histone H3,^[72,73] and aurora B kinase.^[7,74] In

brief, CMs were treated with NPs concentrations corresponding to 1×10^{-6} , 3×10^{-6} , 5×10^{-6} , and 10×10^{-6} M of CHIR99021 (concentrations of SB were approximately double), calculated from the LD values of the NPs and corresponding to a safe dose of NPs. The biological effect was then evaluated by immunostainings, quantifying the intensity of the selected markers in the nuclei (**Figure 8A**). DAPI staining was used to identify the nuclear area.

The encapsulation of the Wnt activator CHIR99021, and the p38 MAPK inhibitor, SB203580, in AcDXSp NPs coated with TA induced an increase of both Ki67 (**Figure 8B**) and phospho-histone H3 (**Figure 8C**) positive nuclei in a concentration-dependent manner. Empty NPs, showed an inhibitory effect instead, demonstrating the importance of the selected compounds in the pro-proliferative effect. Since

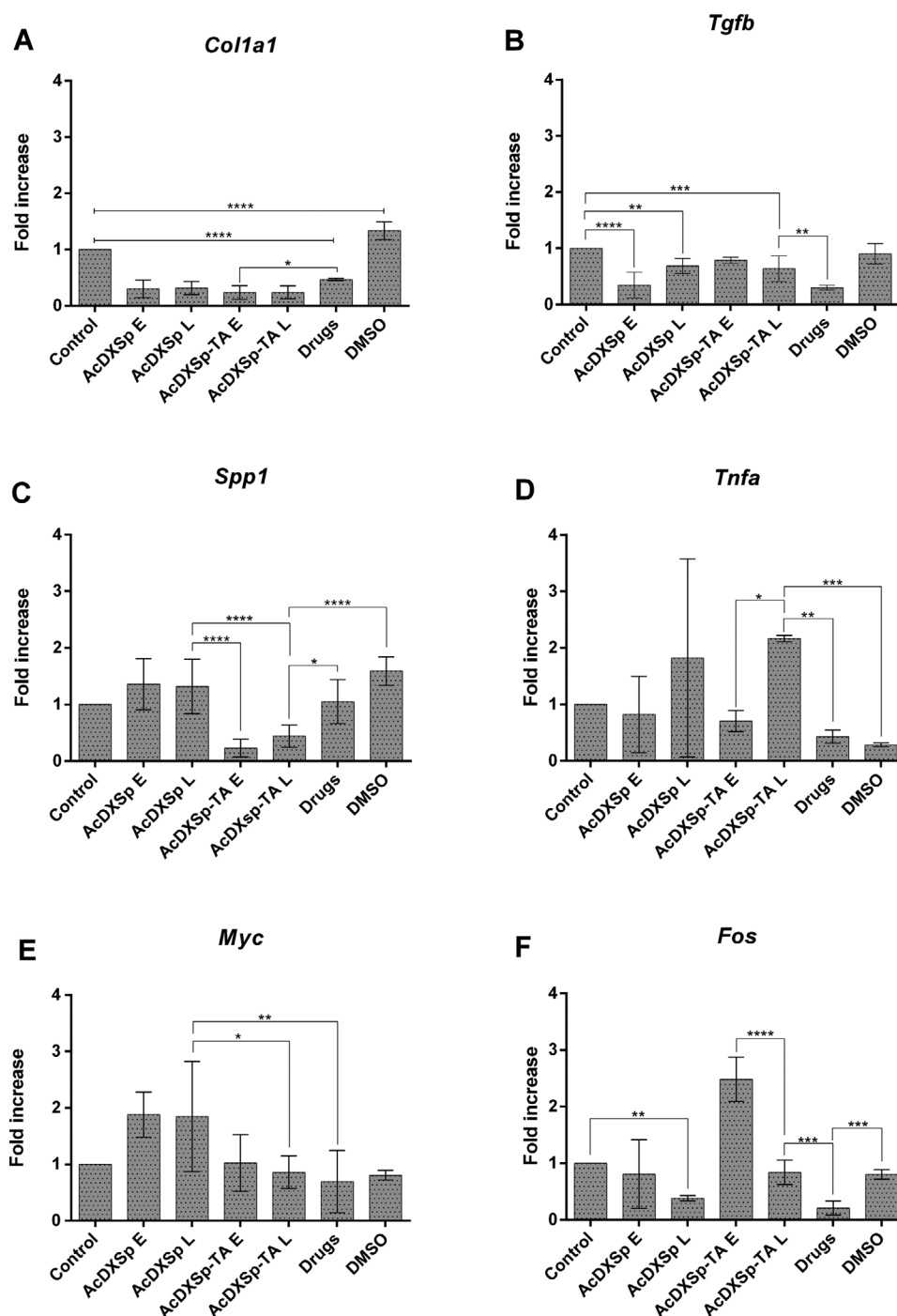


Figure 7. Evaluation of expression of pro-fibrotic genes by RT-qPCR. The anti-fibrotic properties of the TA coating have been evaluated with both empty (E) and drugs loaded NPs (L), by quantification of the expression of pro-fibrotic genes, such as A) Col1a1, B) Tgfb, C) Spp1, D) Tnfa (D), E) Myc and F) Fos. Results are represented as fold increase values compared to the control \pm s.d. ($n = 3$ biological replicates in which each time three technical replicates have been used). A one-way ANOVA followed by a Tukey–Kramer post hoc test was used for the statistical analysis. The significance levels of the differences in uptake studies were set at the probabilities of $*p < 0.05$, $**p < 0.01$, $***p < 0.001$, and $****p < 0.0001$ for comparison with the medium, which was used as control, with the compounds alone, with loaded AcDXSp NPs and with DMSO.

Ki67 is a proliferation marker for cells in active cell cycle, and phospho-histone H3 is a mitotic index marker, such observations are suggestive that drug-loaded TA-coated AcDXSp NPs stimulate cell cycle re-entry of the primary CMs.

We next performed the same Ki67 staining also in human induced pluripotent stem cells (hiPSC)-CMs to confirm the effect in cells of different origin. Also for hiPSC-CMs, the treatment with AcDXSp-TA NPs increased Ki67 (Figure S7,

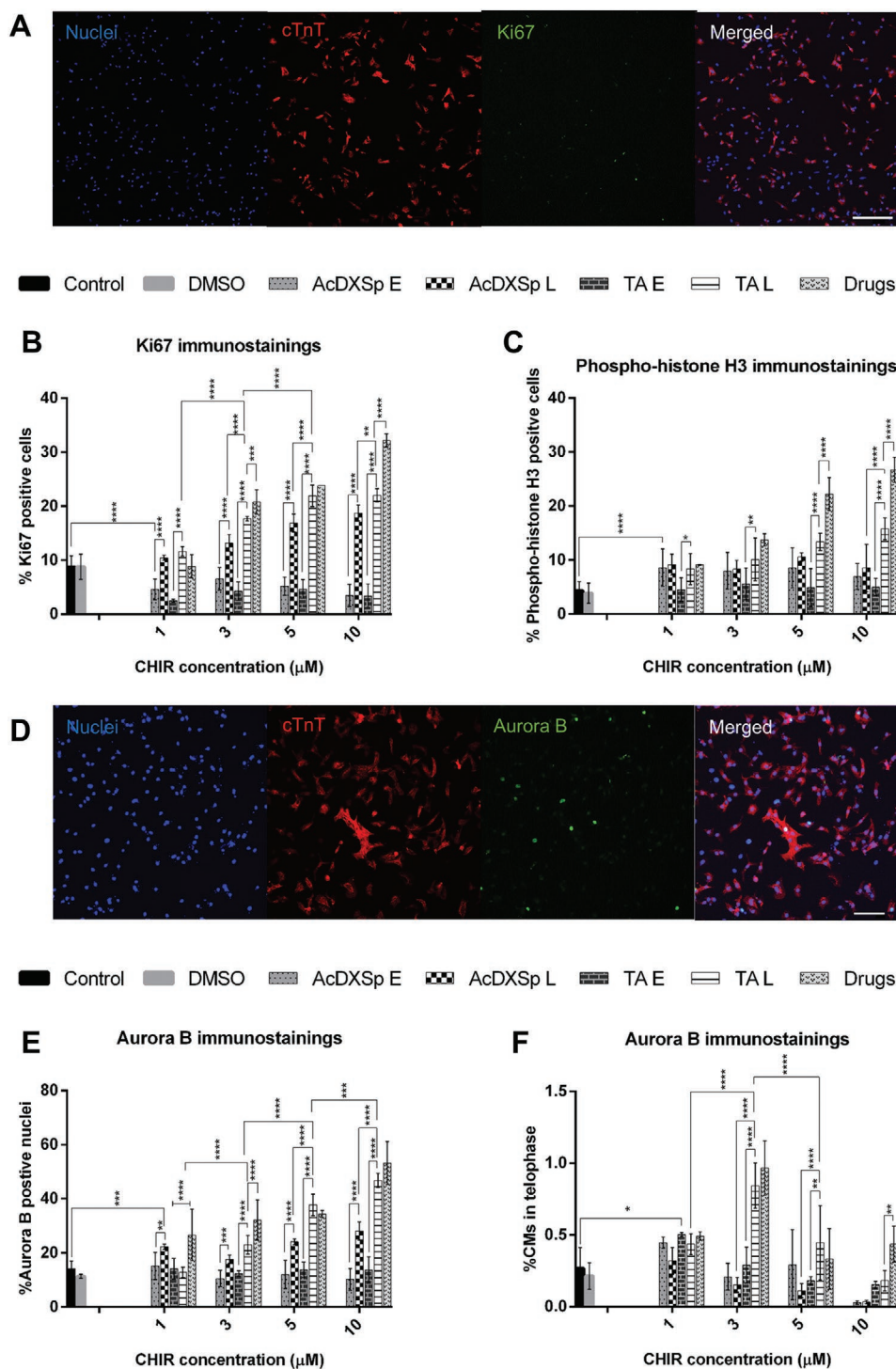


Figure 8. High-content cell imaging and quantification of Ki67, phospho-histone H3, and aurora B staining intensity. Representative images of A) CMs treated with empty (E) and loaded (L) AcDXSp-TA NPs at the concentrations of 1×10^{-6} M of CHIR99021 and 2.2×10^{-6} M of SB203580, and stained for nuclei (DAPI, blue), cardiac troponin T (cTnT, red) and Ki67 (green), with a $10 \times$ magnification objective. Scale bars are $200 \mu\text{m}$. Quantification of B) Ki67 and C) phospho-histone H3 staining intensity in the nucleus. Representative images of D) CMs treated with loaded AcDXSp-TA NPs at the dose of 1×10^{-6} M of CHIR99021 and 2.2×10^{-6} M of SB203580, and stained for nuclei (DAPI, blue), cardiac troponin T (cTnT, red) and aurora B (green), with a $20 \times$ magnification objective. Scale bars are $100 \mu\text{m}$. Quantification of aurora B staining intensity in E) the nucleus and F) percentage of CMs in telophase. The different treatment conditions are stated in the legend. Values represent the mean \pm s.d. ($n = 3$). A one-way ANOVA followed by a Tukey-Kramer post hoc test was used for the statistical analysis. The significance levels of the differences were set at the probabilities of $*p < 0.05$, $**p < 0.01$, $***p < 0.001$, and $****p < 0.0001$ for comparison with the medium, which was used as control, with the compounds alone, between empty and loaded NPs, as well as bare and TA coated NPs.

Supporting Information) in the nuclei, showing that the system has a proliferative effect also on CMs of human origin.

For aurora B, the staining has a nuclear localization when a cell enters the cell cycle and is in interphase or prophase.^[75] When the cell cycle progresses, the cellular localization of aurora B changes, allowing to distinguish in which phase of the cell cycle a cell is (Figure 8D).^[75] In our study, we first quantified the percentage of aurora B positive nuclei (Figure 8E), and demonstrated that drug-loaded TA-coated NPs increase nuclear positivity in a concentration-dependent manner. This further confirmed that the drug-loaded TA-coated NPs successfully stimulate CMs to enter the cell cycle. However, it is known that despite being able to enter the cell cycle, CMs might not physically divide, i.e., complete cytokinesis, giving origin to bi-/polynucleated cells.^[76] In order to evaluate whether the NPs induced cell division, we performed a double-blinded study and manually counted the cells that were in telophase to quantify cytokinesis. Figure 8F and Figure S8 (Supporting Information) show that when cells were treated with drug-loaded TA-coated NPs (Figure S8C, Supporting Information), a higher percentage of cells in cytokinesis was observed. In particular, at the concentration of CHIR of 3×10^{-6} M, the delivery of the compounds CHIR and SB doubled the percentage of dividing CMs compared to the control (Figure 8 and Figure S8A, Supporting Information).

Furthermore, we also measured the surface area of the cells since when a cell enters mitosis, its relative surface area decreases due to a rounding-up phase.^[77] The analysis supported (Figure S9, Supporting Information) that CMs were dividing when treated with drug-loaded TA-coated NPs, as reflected by the smaller mean surface area of the cells when compared to the ones that received other treatments.

Finally, we performed the quantification of cyclins by RT-qPCR to investigate how proliferation was modulated in CMs. Cyclin D triggers cells to move from G₀ to G₁ phase by activating Cdk4 and/or Cdk6.^[78,79] Cyclin E activates Cdk2 and prepares the cell for DNA replication, making them enter the S phase.^[78,79] Cyclin A is synthesized at the onset of S phase and activates the DNA replication inside the nucleus.^[80,81] Also, the interaction between Cdk1 and cyclin A activity is required for the initiation of prophase.^[82] Cyclin B also promotes the assembly of the mitotic spindle and complexed Cdk1/cyclin B actively participates in complete mitosis.^[83] As shown in Figure S10A (Supporting Information), the loading of the compounds C and S in AcDXSp-TA NPs increased the expression of cyclin D in cells, compared to treatment with empty TA-coated NPs, showing that the compounds stimulate cells to enter the cell cycle. The same trend is shown for cyclin E (Figure S10B, Supporting Information), cyclin A (Figure S10C, Supporting Information), and cyclin B (Figure S10D, Supporting Information), showing that the drug-loaded TA-coated NPs promote cell cycle entry and progression in CMs. In particular, the increased expression of cyclin B in cells treated with drug-loaded TA-AcDXSp NPs demonstrates that the compounds encapsulated are able to induce CMs through mitosis.

Overall, CHIR99021 and SB203580 have shown to synergistically promote CMs proliferation. However, due to their poor bioavailability and potential toxic off-target effects, their clinical

translation is still inexistent. Our results show that the developed nanosystem is able to stimulate the proliferation of CMs in vitro, which is important when aiming at the regeneration of the cardiac tissue. The drug compounds encapsulated in the NPs, CHIR, and SB, have also been demonstrated in literature with the ability to regulate the response of inflammatory cells and promote the switch to an anti-inflammatory phenotype.^[66–70] This secondary therapeutic effect could be exploited to reduce the inflammation taking place after a MI and that is negatively affecting the heart remodeling. Moreover, the combination with the anti-fibrotic properties of TA-coated AcDXSp NPs could further contrast the fibrosis taking place after MI and lead to the regeneration of the cardiac tissue.

4. Conclusion

In this work, in order to achieve regeneration of the infarcted heart, two small hydrophobic compounds, CHIR99021 and SB203580, were encapsulated in the pH-responsive polymer AcDXSp for the stimulation of CMs proliferation. The coating of the system with TA allowed a fast and easy surface modification of the NPs, improved cell biocompatibility and stability of the system, and provided heart targeting properties, due to the affinity of the polyphenol for components of the ECM, abundant in the infarcted myocardium. The TA-coated NPs were also taken up preferentially by CMs, which showed a two-fold higher MFI value compared to uncoated NPs. The TA coating showed also anti-fibrotic properties, inducing more than an 80% reduction of expression in genes such as Col1a1 and osteopontin. This could have significant potential in inhibition of the cardiac remodeling, especially when combined with the proliferative properties of the encapsulated compounds, which allowed to double the percentage of CMs dividing compared to the control. Overall, as a proof-of-concept, here we investigated the therapeutic potential of TA-coated AcDXSp NPs, which allowed successfully deliver two drug compounds for cardiac proliferation in CMs. The synergistic anti-fibrotic effect of the TA together with the reported anti-inflammatory effects of the drugs, hold potential for the treatment of HF. The system could encapsulate also different drug molecules and miRNAs, providing a nanoplatform for combination therapies.

Supporting Information

Supporting Information is available from the Wiley Online Library or from the author.

Acknowledgements

V.B. is an employee at Bayer Oy (Finland). V.B. acknowledges University of Helsinki Research Funds. H.A.S. acknowledges financial support from the Sigrid Jusélius Foundation and the Academy of Finland (grant no. 317042). H.R. acknowledges the financial support from the Sigrid Jusélius Foundation and the Finnish Foundation of Cardiovascular Research. M.-A.S. acknowledges financial support from the Academy of Finland (grant no. 317316). V.T. acknowledges financial support from the Academy of Finland (grant no. 321564) and the Finnish Foundation for Cardiovascular Research. The authors also acknowledge the following

core facilities funded by Biocenter Finland: Electron Microscopy Unity of the University for providing the facilities for TEM imaging, Flow cytometry, MST, and Biacore core facilities of the University for the flow cytometer and the Light Microscopy Unit of the Institute of Biotechnology for the confocal microscope and the high-content imaging platform.

Conflict of Interest

Dr. V. Balasubramanian is an employee at Bayer Oy (Finland). The other authors declare that they have no known competing financial interests or personal relationships that could have appeared to influence the work reported in this paper.

Data Availability Statement

Research data are not shared.

Keywords

cardiac regeneration, fibrosis, heart targeting, proliferation, spermine-acetalated dextran nanoparticles, tannic acid

Received: September 7, 2021

Revised: October 3, 2021

Published online: October 22, 2021

- [1] GBD 2017, *Causes of Death Collaborators, Lancet* **2018**, 392, 1736.
- [2] A. Uygun, R. T. Lee, *Dev. Cell* **2016**, 36, 362.
- [3] V. Talman, H. Ruskoaho, *Cell Tissue Res.* **2016**, 365, 563.
- [4] S. M. G. St. John, S. Norman, *Circulation* **2000**, 101, 2981.
- [5] A. P. Ambrosy, G. C. Fonarow, J. Butler, O. Chioncel, S. J. Greene, M. Vaduganathan, S. Nodari, C. S. P. Lam, N. Sato, A. N. Shah, M. Gheorghiu, *J. Am. Coll. Cardiol.* **2014**, 63, 1123.
- [6] H. Uosaki, A. Magadum, K. Seo, H. Fukushima, A. Takeuchi, Y. Nakagawa, K. W. Moyes, G. Narazaki, K. Kuwahara, M. Lafamme, S. Matsuoka, N. Nakatsuji, K. Nakao, C. Kwon, D. A. Kass, F. B. Engel, J. K. Yamashita, *Circ.: Cardiovasc. Genet.* **2013**, 6, 624.
- [7] F. B. Engel, M. Schebesta, M. T. Duong, G. Lu, S. Ren, J. B. Madwed, H. Jiang, Y. Wang, M. T. Keating, *Genes Dev.* **2005**, 19, 1175.
- [8] S. Gessert, M. Kühl, *Circ. Res.* **2010**, 107, 186.
- [9] G. Ozhan, G. Weidinger, *Cell Regener.* **2015**, 4, 4:3.
- [10] D. M. Titmarsh, N. R. Glass, R. J. Mills, A. Hidalgo, E. J. Wolvetang, E. R. Porrello, J. E. Hudson, J. J. Cooper-White, *Sci. Rep.* **2016**, 6, 24637.
- [11] Z. Lin, W. T. Pu, *Sci. Transl. Med.* **2014**, 6, 239rv1.
- [12] K. Gabisonia, G. Prosdocimo, G. D. Aquaro, L. Carlucci, L. Zentilin, I. Secco, H. Ali, L. Braga, N. Gorgodze, F. Bernini, S. Burchielli, C. Collesi, L. Zandonà, G. Sinagra, M. Piacenti, S. Zaccagna, R. Bussani, F. A. Recchia, M. Giacca, *Nature* **2019**, 569, 418.
- [13] C. L. Ventola, *P T* **2012**, 37, 512.
- [14] S. Kargozar, M. Mozafari, *Mater. Today: Proc.* **2018**, 5, 15492.
- [15] T. Dvir, M. Bauer, A. Schroeder, J. H. Tsui, D. G. Anderson, R. Langer, R. Liao, D. S. Kohane, *Nano Lett.* **2011**, 11, 4411.
- [16] R. C. Scott, J. M. Rosano, Z. Ivanov, B. Wang, P. L.-G. Chong, A. C. Issekutz, D. L. Crabbe, M. F. Kiani, *FASEB J.* **2009**, 23, 3361.
- [17] M. P. A. Ferreira, S. Ranjan, S. Kinnunen, A. Correia, V. Talman, E. Mäkilä, B. Barrios-Lopez, M. Kemell, V. Balasubramanian, J. Salonen, J. Hirvonen, H. Ruskoaho, A. J. Airaksinen, H. A. Santos, *Small* **2017**, 13, 1701276.
- [18] G. Torrieri, F. Fontana, P. Figueiredo, Z. Liu, M. P. A. Ferreira, V. Talman, J. P. Martins, M. Fusciello, K. Moslova, T. Teesalu, V. Cerullo, J. Hirvonen, H. Ruskoaho, V. Balasubramanian, H. A. Santos, *Nanoscale* **2020**, 12, 2350.
- [19] M. P. A. Ferreira, S. Ranjan, A. M. R. Correia, E. M. Mäkilä, S. M. Kinnunen, H. Zhang, M.-A. Shahbazi, P. V. Almeida, J. J. Salonen, H. J. Ruskoaho, A. J. Airaksinen, J. T. Hirvonen, H. A. Santos, *Biomaterials* **2016**, 94, 93.
- [20] H. Takahama, T. Minamino, H. Asanuma, M. Fujita, T. Asai, M. Wakeno, H. Sasaki, H. Kikuchi, K. Hashimoto, N. Oku, M. Asakura, J. Kim, S. Takashima, K. Komamura, M. Sugimachi, N. Mochizuki, M. Kitakaze, *J. Am. Coll. Cardiol.* **2009**, 53, 709.
- [21] M. Galagudza, D. Korolev, V. Postnov, E. Naumisheva, Y. Grigороva, I. Uskov, E. Shlyakhto, *Int. J. Nanomed.* **2012**, 7, 1671.
- [22] M. M. Nguyen, A. S. Carlini, M.-P. Chien, S. Sonnenberg, C. Luo, R. L. Braden, K. G. Osborn, Y. Li, N. C. Gianneschi, K. L. Christman, *Adv. Mater.* **2015**, 27, 5547.
- [23] M. Liu, M. Li, S. Sun, B. Li, D. Du, J. Sun, F. Cao, H. Li, F. Jia, T. Wang, N. Chang, H. Yu, Q. Wang, H. Peng, *Biomaterials* **2014**, 35, 3697.
- [24] Y. T. Ko, W. C. Hartner, A. Kale, V. P. Torchilin, *Gene Ther.* **2009**, 16, 52.
- [25] M. P. A. Ferreira, V. Talman, G. Torrieri, D. Liu, G. Marques, K. Moslova, Z. Liu, J. F. Pinto, J. Hirvonen, H. Ruskoaho, H. A. Santos, *Adv. Funct. Mater.* **2018**, 28, 1705134.
- [26] M. Shin, H.-A. Lee, M. Lee, Y. Shin, J.-J. Song, S.-W. Kang, D.-H. Nam, E. J. Jeon, M. Cho, M. Do, S. Park, M. S. Lee, J.-H. Jang, S.-W. Cho, K.-S. Kim, H. Lee, *Nat. Biomed. Eng.* **2018**, 2, 304.
- [27] J. Guo, Y. Ping, H. Ejima, K. Alt, M. Meissner, J. J. Richardson, Y. Yan, K. Peter, D. von Elverfeldt, C. E. Hagemeyer, F. Caruso, *Angew. Chem.* **2014**, 126, 5579.
- [28] H. Ejima, J. J. Richardson, K. Liang, J. P. Best, M. P. van Koevorden, G. K. Such, J. Cui, F. Caruso, *Science* **2013**, 341, 154 LP.
- [29] A. Andersen, Y. Chen, H. Birkedal, *Biomimetics* **2019**, 4, 30.
- [30] S. Krungchanuchat, T. Thongtem, S. Thongtem, C. Pilapong, *Bioinert-phases* **2017**, 12, 021005.
- [31] A. Mero, T. Ishino, I. Chaiken, F. M. Veronese, G. Pasut, *Pharm. Res.* **2011**, 28, 2412.
- [32] M. I. Setyawati, C. Y. Tay, D. Docter, R. H. Stauber, D. T. Leong, *Chem. Soc. Rev.* **2015**, 44, 8174.
- [33] J. R. Aguilera, V. Venegas, J. M. Oliva, M. J. Sayagués, M. de Miguel, J. A. Sánchez-Alcázar, M. Arévalo-Rodríguez, A. P. Zaderenko, *RSC Adv.* **2016**, 6, 7279.
- [34] E. A. Ainsworth, K. M. Gillespie, *Nat. Protoc.* **2007**, 2, 875.
- [35] J. Woods, M. Mellon, *Ind. Eng. Chem., Anal. Ed.* **1941**, 13, 551.
- [36] L. Kou, J. Sun, Y. Zhai, Z. He, *Asian J. Pharm. Sci.* **2013**, 8, 1.
- [37] A.-S. Tseng, F. B. Engel, M. T. Keating, *Chem. Biol.* **2006**, 13, 957.
- [38] T. T. Beaudette, J. A. Cohen, E. M. Bachelder, K. E. Broaders, J. L. Cohen, E. G. Engleman, J. M. J. Fréchet, *J. Am. Chem. Soc.* **2009**, 131, 10360.
- [39] E. R. Gillies, A. P. Goodwin, J. M. J. Fréchet, *Bioconjugate Chem.* **2004**, 15, 1254.
- [40] E. M. Bachelder, E. N. Pino, K. M. Ainslie, *Chem. Rev.* **2017**, 117, 1915.
- [41] P. B. Garlick, G. K. Radda, P. J. Seeley, *Biochem. J.* **1979**, 184, 547.
- [42] K. R. Khabbaz, F. Zankoul, K. G. Warner, *Ann. Thorac. Surg.* **2001**, 72, S2227.
- [43] S. L. Suarez, A. Muñoz, A. Mitchell, R. L. Braden, C. Luo, J. R. Cochran, A. Almutairi, K. L. Christman, *ACS Biomater. Sci. Eng.* **2016**, 2, 197.
- [44] H. A. Santos, J. Riikonen, J. Salonen, E. Mäkilä, T. Heikkilä, T. Laaksonen, L. Peltonen, V.-P. Lehto, J. Hirvonen, *Acta Biomater.* **2010**, 6, 2721.
- [45] Y. Fan, B. X. Ho, J. K. S. Pang, N. M. Q. Pek, J. H. Hor, S.-Y. Ng, B.-S. Soh, *Stem Cell Res. Ther.* **2018**, 9, 338.

- [46] E. Fröhlich, *Int. J. Nanomed.* **2012**, *7*, 5577.
- [47] E. B. Reed, S. Ard, J. La, C. Y. Park, L. Culligan, J. J. Fredberg, L. V. Smolyaninova, S. N. Orlov, B. Chen, R. Guzy, G. M. Mutlu, N. O. Dulin, *Respir. Res.* **2019**, *20*, 168.
- [48] X. Chu, H. Wang, Y. Jiang, Y. Zhang, Y. Bao, X. Zhang, J. Zhang, H. Guo, F. Yang, Y. Luan, Y. Dong, *J. Pharmacol. Sci.* **2016**, *130*, 15.
- [49] J. A. Cooper, *J. Cell Biol.* **1987**, *105*, 1473 LP.
- [50] D. A. Kuhn, D. Vanhecke, B. Michen, F. Blank, P. Gehr, A. Petri-Fink, B. Rothen-Rutishauser, *Beilstein J. Nanotechnol.* **2014**, *5*, 1625.
- [51] T. dos Santos, J. Varela, I. Lynch, A. Salvati, K. A. Dawson, *PLoS One* **2011**, *6*, e24438.
- [52] L. Thors, J. Eriksson, C. J. Fowler, *Br. J. Pharmacol.* **2007**, *152*, 744.
- [53] K. H. Sit, B. H. Bay, K. P. Wong, *In Vitro Cell. Dev. Biol.: Anim.* **1993**, *29*, 395.
- [54] Z. M. Qian, H. Li, H. Sun, K. Ho, *Pharmacol. Rev.* **2002**, *54*, 561 LP.
- [55] J. N. Stannard, B. L. Horecker, *J. Biol. Chem.* **1948**, *172*, 599.
- [56] M. C. Bennett, G. W. Mlady, M. Fleshner, G. M. Rose, *Proc. Natl. Acad. Sci. USA* **1996**, *93*, 1330.
- [57] M. Bujak, N. G. Frangogiannis, *Cardiovasc. Res.* **2007**, *74*, 184.
- [58] D. Ma, B. Zheng, H. Du, X. Han, X. Zhang, J. Zhang, Y. Gao, S. Sun, L. Chu, *Front. Pharmacol.* **2020**, *11*, 716.
- [59] X. Hua, Y.-Y. Wang, P. Jia, Q. Xiong, Y. Hu, Y. Chang, S. Lai, Y. Xu, Z. Zhao, J. Song, *BMC Med.* **2020**, *18*, 2.
- [60] H. Khalil, O. Kanisicak, V. Prasad, R. N. Correll, X. Fu, T. Schips, R. J. Vagnozzi, R. Liu, T. Huynh, S.-J. Lee, J. Karch, J. D. Molckentin, *J. Clin. Invest.* **2017**, *127*, 3770.
- [61] Y. Matsui, N. Jia, H. Okamoto, S. Kon, H. Onozuka, M. Akino, L. Liu, J. Morimoto, S. R. Rittling, D. Denhardt, A. Kitabatake, T. Uede, *Hypertension* **2004**, *43*, 1195.
- [62] X. Palomer, M. S. Román-Azcona, J. Pizarro-Delgado, A. Planavila, F. Villarroya, B. Valenzuela-Alcaraz, F. Crispi, Á. Sepúlveda-Martínez, I. Miguel-Escalada, J. Ferrer, J. F. Nistal, R. García, M. M. Davidson, E. Barroso, M. Vázquez-Carrera, *Signal Transduction Targeted Ther.* **2020**, *5*, 14.
- [63] C. Duerrschmid, J. Trial, Y. Wang, M. L. Entman, S. B. Haudek, *Circ.: Heart Failure* **2015**, *8*, 352.
- [64] J. Yeo, J. Lee, S. Yoon, W. J. Kim, *Biomater. Sci.* **2020**, *8*, 1148.
- [65] Y. Wu, L. Zhong, Z. Yu, J. Qi, *Drug Dev. Res.* **2019**, *80*, 262.
- [66] Q. Shi, L. Cheng, Z. Liu, K. Hu, J. Ran, D. Ge, J. Fu, *Cent. Eur. J. Immunol.* **2015**, *40*, 276.
- [67] L. Wang, Y. Wang, C. Zhang, J. Li, Y. Meng, M. Dou, C. T. Noguchi, L. Di, *Arterioscler., Thromb., Vasc. Biol.* **2018**, *38*, 2103.
- [68] D. Sorcini, S. Bruscoli, T. Frammartino, M. Cimino, E. Mazzon, M. Galuppo, P. Bramanti, M. Al-Banchaabouchi, D. Farley, O. Ermakova, O. Britanova, M. Izraelson, D. Chudakov, M. Biagioli, P. Sportoletti, S. Flamini, M. Raspa, F. Scavizzi, C. Nerlov, G. Migliorati, C. Riccardi, O. Bereshchenko, *J. Immunol.* **2017**, *199*, 3031.
- [69] D. Yang, W. Fu, L. Li, X. Xia, Q. Liao, R. Yue, H. Chen, X. Chen, S. An, C. Zeng, W. E. Wang, *Clin. Sci.* **2017**, *131*, 2919.
- [70] J. O. Abaricia, A. H. Shah, M. Chaubal, K. M. Hotchkiss, R. Olivares-Navarrete, *Biomaterials* **2020**, *243*, 119920.
- [71] C. Feliciani, E. Ruocco, A. Zampetti, P. Toto, P. A. Amerio, A. Tulli, P. Amerio, V. Ruocco, *Int. J. Immunopathol. Pharmacol.* **2007**, *20*, 289.
- [72] V. Villani, K. K. Mahadevan, M. Ligorio, C. Fernández-del Castillo, D. T. Ting, F. Sabbatino, I. Zhang, M. Vangel, S. Ferrone, A. L. Warshaw, K. D. Lillemoe, J. Wargo, V. Deshpande, C. R. Ferrone, *Ann. Surg. Oncol.* **2016**, *23*, 609.
- [73] M. J. Hendzel, Y. Wei, M. A. Mancini, A. Van Hooser, T. Ranalli, B. R. Brinkley, D. P. Bazett-Jones, C. D. Allis, *Chromosoma* **1997**, *106*, 348.
- [74] Q. Wu, W. Zhang, T. Mu, T. Song, D. Li, *Cell Biol. Int.* **2013**, *37*, 436.
- [75] C. Crosio, G. M. Fimia, R. Loury, M. Kimura, Y. Okano, H. Zhou, S. Sen, C. D. Allis, P. Sassone-Corsi, *Mol. Cell. Biol.* **2002**, *22*, 874.
- [76] M. Leone, A. Magadum, F. B. Engel, *Am. J. Physiol.: Heart Circ. Physiol.* **2015**, *309*, H1237.
- [77] A. G. Clark, E. Paluch, in *Cell Cycle in Development* (Ed: J. Z. Kubiak), Springer, Berlin **2011**, Ch. 3.
- [78] C. J. Sherr, J. M. Roberts, *Genes Dev.* **1999**, *13*, 1501.
- [79] C. J. Sherr, J. M. Roberts, *Genes Dev.* **2004**, *18*, 2699.
- [80] B. O. Petersen, J. Lukas, C. S. Sørensen, J. Bartek, K. Helin, *EMBO J.* **1999**, *18*, 396.
- [81] D. Coverley, C. Pelizon, S. Trewick, R. A. Laskey, *J. Cell Sci.* **2000**, *113*, 1929.
- [82] N. Furuno, N. den Elzen, J. Pines, *J. Cell Biol.* **1999**, *147*, 295.
- [83] K. Riabowol, G. Draetta, L. Brizuela, D. Vandre, D. Beach, *Cell* **1989**, *57*, 393.